# Design Optimization and Analysis of Coated Particle Fuel Using Advanced Fuel Performance Modeling Techniques

**Jing Wang[a], Ronald G. Ballinger[a], Jane T. Diecker[a]**
([a]MIT Nuclear Engineering Department, 185 Albany Street, Cambridge, MA, 02139, USA)

## ABSTRACT

TIMCOAT, an advanced fuel performance model for coated particle fuel, has has been used to optimize coated particle fuel design with respect to end of life failure probability. TIMCOAT is an integrated fuel performance model for coated particle fuel that has been developed to comprehensively study the behavior of TRISO coated fuel. Modeling of both pebble bed and prismatic configurations is possible. Monte Carlo sampling of particles is employed in fuel failure prediction to capture the statistical features of dimensions, material properties, and in the case of the pebble bed concept, the statistical nature of the refueling process. The model has been used to optimize fuel reliability with respect to initial dimensions and physical properties and the uncertainty in the values for these properties for two pebble bed core designs, one with an un-fueled central pebble column and another with a solid graphite central column . In addition, the effect of uncertainties in fuel particle dimensions and physical properties has been explored.

## 1.0 INTRODUCTION

Superior, and predictable, coated particle fuel performance will be essential for the development and deployment of gas cooled reactor systems for future power generation. Unfortunately, unlike light water reactor (LWR) type fuel, which can undergo 100% inspection of all individual components as well as the finished fuel element, coated particle fuel cannot be inspected in detail other than to identify clearly failed particles, those which do not meet overall dimensional specifications or contain no fuel. For this reason, the modeling of both the fabrication process and the in-reactor performance will play a critical role in the establishment of the safety case for this type of fuel. The achievement of high reliability will require a significant development effort in a number of areas including: (1) coated particle fuel process development and manufacture, (2) in-pile testing, and (3) modeling of the overall system. Fuel performance modeling can serve as a means to develop better understanding of irradiation testing, point to improved process development, and reduce the overall development cost through a reduction in required expensive irradiation testing. However, the behavior of the coated particle fuel system is a function of many variables, several of which are not easily measurable. Additionally, the complexity of the interaction between components of an individual coated particle and the thermal environment during exposure can lead to counterintuitive behavior especially when attempting to evaluate the thermal and irradiation induced stresses that can lead to particle failure. Moreover, the development of a optimized coated particle design will require knowledge of the relationship between processing parameters, subsequent physical properties and dimensions. Lastly, the statistical nature of the coated particle fabrication process, which leads to statistical distributions for many of the as fabricated dimensions and physical properties, will result in a distribution of resulting behavior and hence a distribution in particle reliability-failure probability. In order to assure reliable behavior it will be critical that insight into the optimization process be developed. Fuel performance modeling can play a key role in the optimization process and can help bridge the gap between what can be measured and what cannot. To this end new models are being developed, among which is a model, TIMCOAT, being developed at MIT [1-4] A detailed description of the initial version of the model has been reported elsewhere [3]. In this paper we present initial results concerning the effect of in-core exposure history and fabrication variables on the reliability of coated particle fuel. In particular, we focus on the pebble bed reactor design in which coated particle fuel is passed through the core several times during design life as opposed to exposure in

prismatic (block) type cores where the fuel remains stationary. The current version of the model deals only with mechanical failure of the particle due to fracture of the kernel coatings. Thus, failure by non-mechanical processes, which may be significant for some conditions, will not be treated in this analysis. In this analysis we focus on the following areas: (1) the effect of power history and core power distribution on fuel reliability and (2) the effect of uncertainty in as-fabricated fuel properties on fuel reliability.

## 2.0 COATED PARTICLE FUEL MECHANICAL RESPONSE TO IRRADIATION EXPOSURE

Figures 1 and 2 show a schematic of (with typical dimensions shown) and a photograph of an actual coated particle respectively. The most modern gas reactor coated particle fuel design consists of a kernel of fuel, either $UO_2$, UCO, or $PuO_2$, surrounded by a low density pyrocarbon "buffer" layer, and a three-layer structure consisting of an inner dense pyrocarbon, a SiC, and an outer dense pyrocarbon layer.

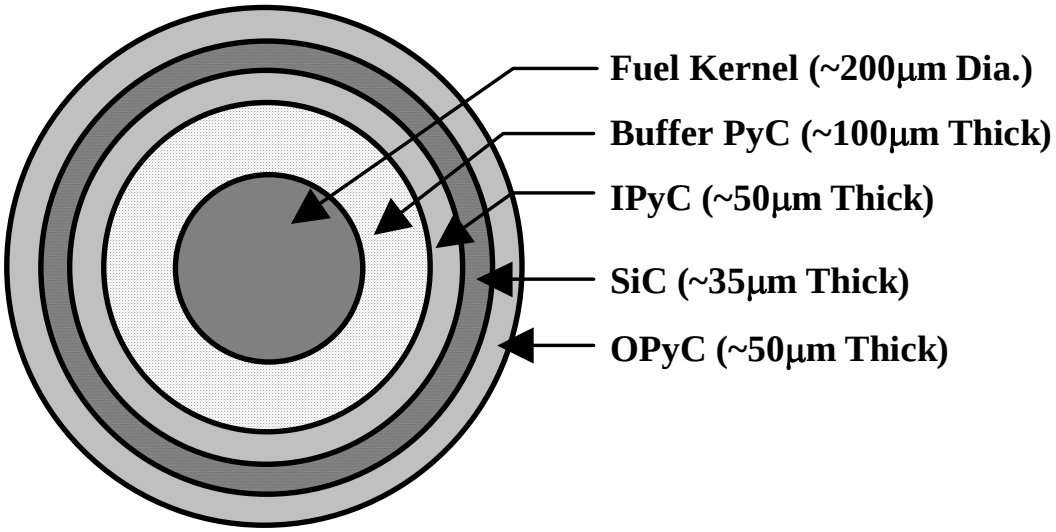


Figure 1. Coated particle fuel schematic.

The buffer layer is of low density and is designed to accommodate swelling and other changes that may occur during operation. The low density also allows for the accommodation of fission gas that is released during operation. Radiation exposure results in significant densification of the buffer. The three layer system, IPyC-SiC-OPyC, forms the primary barrier to fission product release with the SiC layer establishing the main pressure boundary for the particle. During operation the fission process results in the release of fission products to the buffer region. Some of these fission products are gaseous, in particular xenon and krypton. Release of these gases will result in a gradual pressure buildup in the system. Additionally, the presence of graphite in the system will result in pressure buildup from carbon-containing gases ($CO/CO_2$). (At the same time the PyC layers will tend to shrink, putting these layers in circumferential tension and the SiC layer into compression. Eventually both the OPyC and IPyC layers will develop radial cracks and/or circumferential cracks or separations at the PyC/SiC interface. If there were no pyrocarbon layer cracking then the initial stress state of the system would be one of essentially atmospheric pressure within the buffer region and a IPyC-SiC-OPyC stress distribution governed by conditions that existed during the coating process. The coating process is performed by chemical-vapor-

deposition (CVD) in the temperature range 1400-1700°C and can be either be a discontinuous or a continuous or a discontinuous process. In the discontinuous process, used predominantly in the US in the past, the individual layers are deposited in separate coaters with the particles being cooled down between steps. In the continuous process the layers are deposited sequentially using in the same coater by altering the coater environment. The coated particles are then incorporated into the fuel system for the reactor and operated at temperatures in the range of a few hundred C to temperatures approaching the coating temperature. As a result of these processing and operating variables, the initial stress distribution in the barrier layers will not be one of zero initial stress by will be governed by the details of the fabrication process. The pyrocarbon will generally have a higher thermal expansion coefficient than the SiC the initial stress state at room temperature will be one where the pyrocarbon layers will be in slight tension and the SiC layer in slight compression.

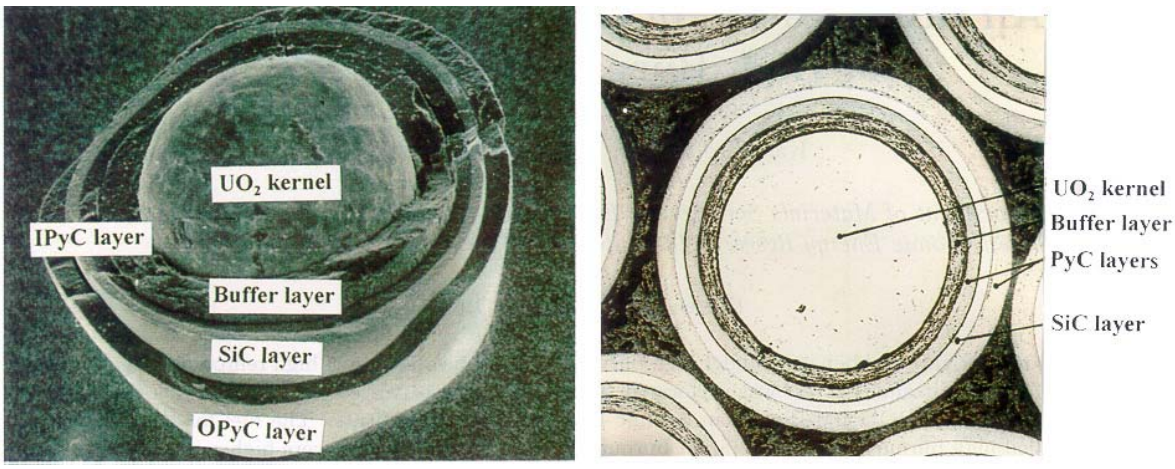


Figure 2. Coated particle fuel showing detailed features [1]

The evolution of stresses in the IPyC-SiC-OPyC layer system during irradiation consists of a slow increase in pressure induced stresses and a much more critical evolution of the stresses due to the irradiation behavior of the pyrocarbon layers. As was pointed out earlier, the ultimate effect of this process is that radial cracking and in some cases circumferential cracking/separation at the pyrocarbon/SiC interface can occur. Subsequent cracking of the SiC layer may occur but will depend on the nature of its interaction with the pyrocarbon layers. Cracking of the pyrocarbon layers will depend on the interaction between irradiation-induced dimensional changes and creep in the pyrocarbon that may relax stresses. This interaction is comples and strongly dependent on temperature, fast neutron fluence, and processing parameters for the pyrocarbon that effect the degree of anisotropy in the graphite structure. The effect of temperature and irradiation are illustrated in figures 3-8.

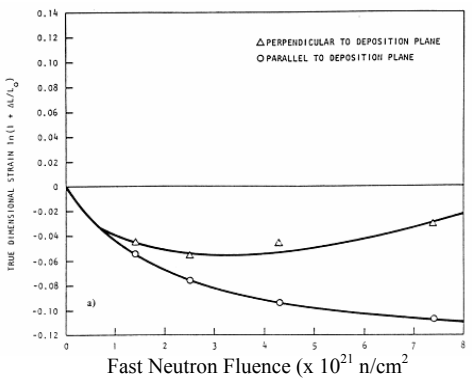


Figure 3. Dimensional changes of low density isotropic pyrolytic carbon during irradiation at 1000°C.

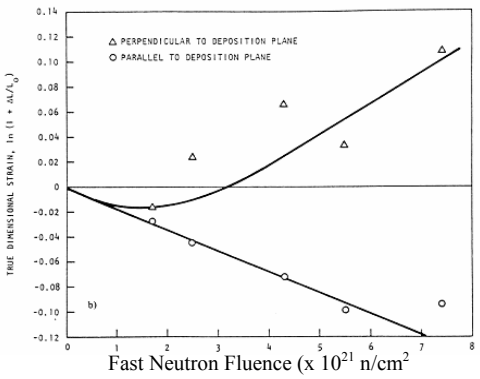


Figure 4. Dimensional changes of high density isotropic pyrolytic carbon during irradiation at 1000°C.

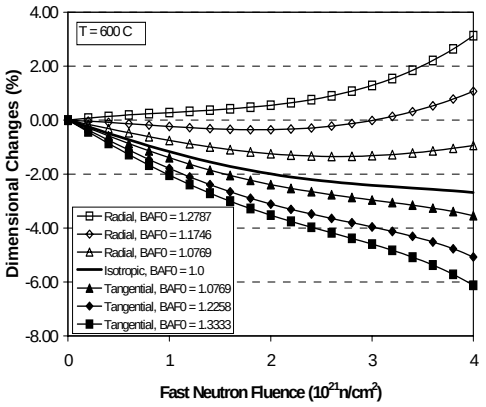


Figure 5. Irradiation induced dimensional changes of pyrolytic carbon , ρ= 1.96 gm/cm$^3$ during irradiation at 600°C*.

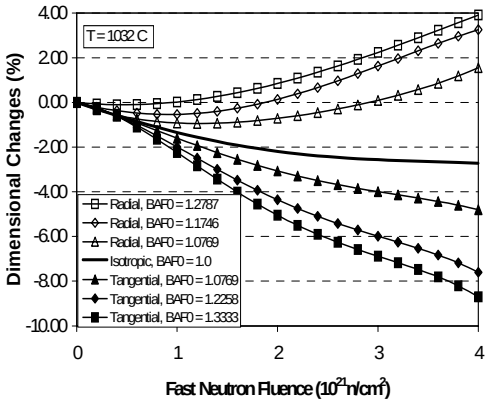


Figure 6. Irradiation induced dimensional changes of pyrolytic carbon , ρ= 1.96 gm/cm$^3$ during irradiation at 1032°C*.

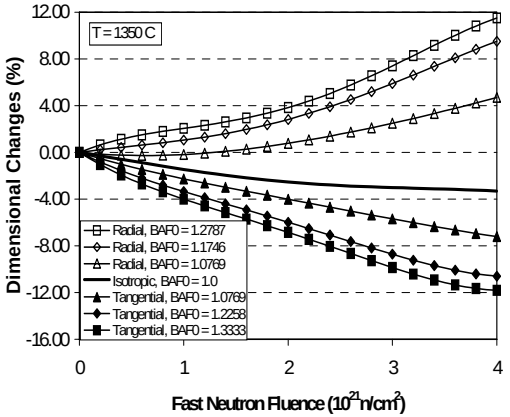


Figure 7. Irradiation induced dimensional changes of pyrolytic carbon , ρ= 1.96 gm/cm$^3$ during irradiation at 1350°C*.

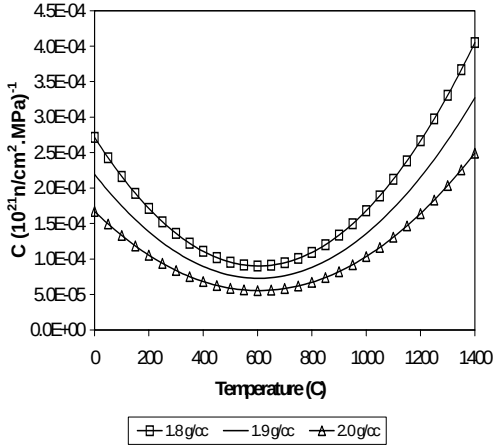


Figure 8. Creep coefficient of pyrocarbon as a function of temperature and density*.

* Symbols in figures 5-8 added for clarity only.

Figures 3 and 4 show the dimensional changes for isotropic pyrocarbon as a function of fluence and density [5]. The pyrocarbon was deposited onto SiC using CVD, The effect of neutron fluence is to first, in most cases, cause shrinkage followed by expansion at higher fluence. The details of the process are complex but the macro effect of the process is to strongly influence the stresses in the surface that the pyrocarbon is bonded to-in our case the SiC barrier layer. Figures 5-7 show the effect of neutron fluence on dimensional changes for non-isotropic pyrocarbons. The degree of anisotropy is represented by the Bacon Anisotropy Factor, $BAF_0$, where the 0 indicates the initial value. The individual crystallites of graphite are highly anisotropic, consistent with their hexagonal crystal structure. If the macro-structure consists of randomly oriented crystallites then the overall macro-structure will be isotropic on average. However, a preferred orientation of the crystallites within the structure will result in global anisotropy of the structure. The BAF represents the degree of anisotropy with values for coated particle pyrocarbon ranging from near 1 (isotropic) to greater than 1.1 (anisotropic). The radiation-induced shrinkage will result in the buildup of tensile circumferential stresses in the pyrocarbon layer when bonded to the SiC layer. In response to this stress buildup, if the temperature is high enough and in the presence of neutron flux, the pyrocarbon stresses will be relaxed due to creep. The creep strain in a given direction can be represented by an equation of the general form:

$$\varepsilon_{cr} = c \cdot (f(\sigma) \cdot \Phi \qquad (1)$$

where:

$f(\sigma)$ is some function of stress and elastic constants
$\Phi$ is the neutron fluence ($n/cm^2$)
c is a steady state creep coefficient.

Figure 8 shows the values for the creep coefficient as a function of temperature and density. As the reader will note, both irradiation-induced shrinkage and creep are non-linear in their behavior and functions of several variables. However, some general characteristics of expected behavior can be noted. First, the shrinkage rate is the highest at low fluences and becomes generally linear with fluence at high fluence. Second, the creep rate will go through a minimum at approximately 600°C and will increase with temperature beyond this. Thus, one would expect that the ability of the system to relax stresses would be the lowest for low fluences, low temperature and for a high degree of anisotropy. The inability to relax stresses will promote cracking to relax these stresses. Thus, pyrocarbon cracking will be promoted for these conditions.

The above discussion related to the evolution of the macro stresses in the system. Figure 9 shows the general trend of the tangential stresses in a typical coated particle irradiated at 1000°C. In general, as mentioned above, the PyC layers are in tension and the SiC layer is in compression throughout the exposure. Eventually the internal fission gas pressure would become high enough to force the SiC layer into tension and failure would occur by overpressure when the fracture strength of the SiC layer is exceeded-the PyC layers having previously cracked.

While the general evolution of stresses is an important consideration for long term exposure, failure can occur at a much earlier exposure due to cracking of the PyC layers followed by failure of the SiC layer due to the development of local tensile stresses at the PyC crack tip/SiC interface. Figure 10 shows a schematic of this behavior. Once the PyC layer cracks, the local stress field at the crack tip can become tensile. The evolution of these stresses has been discussed elsewhere [3]. If the local tensile stress exceeds the fracture toughness, $K_{IC}$ of the SiC then failure by crack initiation from the PyC/SiC interface can occur. Interface separation (failure along the PyC/SiC interface) can also occur but this will not be treated in this discussion. The evolution of the crack-induced failure mechanism proceeds, in general, as follows:

1. One or both of the PyC layers develops radial cracking due to the combination of radiation-induced shrinkage of the PyC constrained by the PyC/SiC bond. The temperature/fluence combination must be in the range where stress relaxation by creep is insufficient to balance the stress buildup.

2. Once a crack initiates in the PyC a stress intensity factor, K, is established at the SiC layer at some microstructural discontinuity at the interface-transferring the stress from the PyC crack tip to the SiC.

3. If the fracture toughness of the SiC is exceeded then SiC cracking occurs and the particle fails.

4. If the fracture toughness is not exceeded then failure does not immediately occur but may occur later. Continued shrinkage of the PyC will continue to produce increasing stresses. If the creep rate is insufficient to relax the stress buildup then failure can occur at higher burnup.

## 3.0 PEBBLE BED REACTOR (PBR): KEY CHARACTERISTICS AND FUELING SCHEME

Pebble-Bed Reactor have received increased interest as one of potential Next Generation Reactor (NGNP) concepts. These concepts show promise for higher efficiency, cost effective, passively safe power generation in the future. The design makes use of a coated particle fuel system that has been described above. The PBR design uses coated fuel particles that are approximately 900 μm in diameter embedded in spherical graphite fuel "pebbles". An individual pebble contains roughly 15,000 coated particles within a graphite matrix in a spherical ball of 6 cm in diameter, which forms the fuel system. For a typical 120MWe reactor core design, there are approximately 360,000 pebbles. The pebbles, unlike the fuel rods in a conventional Light Water Reactor (LWR) which are stationary, move through the core on a continuous basis during operation. Partially burned and fresh fuel, when necessary, is added to the top of the core which has a geometry similar to that of a fluidized packed bed. Fuel pebbles then flow down through the core region. Upon exiting the core after a particular pass the pebbles are checked for accumulated burnup and integrity. Based on the results of this analysis a pebble is either removed from the stream and a new one added or it is recycled to the top (entrance) of the core for another cycle. Heat is transferred from the fuel to a gas, helium in most cases, flowing through the core.

In contrast to the PBR, he Modular Helium Reactor uses a more conventional stationary system in which the fuel particles are embedded in cylindrical fuel "compacts" which are then embedded in graphite fuel blocks. In addition to fuel, the fuel blocks also contain cooling passages and locations for absorber and control material. The MHR is refueled by periodic removal of depleted fuel blocks and the addition of fresh fuel.

While the fuel particle design is identical in form for each of the two systems, the fuel system, moving pebbles vs. prismatic block, results in significant differences in fuel management and thus thermal history. In the pebble bed concept it is possible for a fresh pebble to be "inserted" into a location where the local fission power is also relatively high. This is the result of the random introduction, in terms of ultimate position in the core, of pebbles after a particular pass. As a result, the local peak to average power peaking factor in the fresh pebble can be relatively high compared to the prismatic design for the same nominal thermal conditions. Also, the fission power generated when a highly burned pebble is loaded in the vicinity of several fresh pebbles can "drive" more depleted fuel to higher temperatures than would otherwise be achieved based on its accumulated burnup. On the other hand, the fueling scheme in the stationary prismatic designs results in a steadily decreasing temperature with burnup during exposure due to both the fuel burnup and the fuel management scheme. Additionally, the more favorable heat transfer conditions in the pebble bed core, partially due to a lower power density, results in a peak temperature in the pebble bed design that is often several hundred degrees C lower than the peak temperature in a prismatic core.

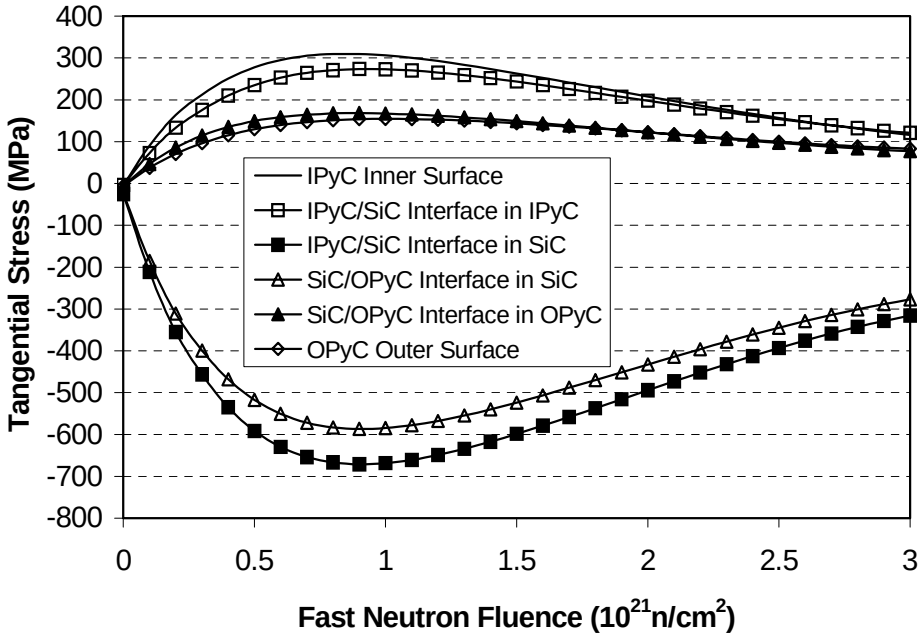


Figure 9. General evolution of tangential stress distribution for a coated particle irradiated at 1000°C The initial PyC density was 1.9 gm/cm$^3$ and the $BAF_0$ was 1.03. Symbols are for clarity only.

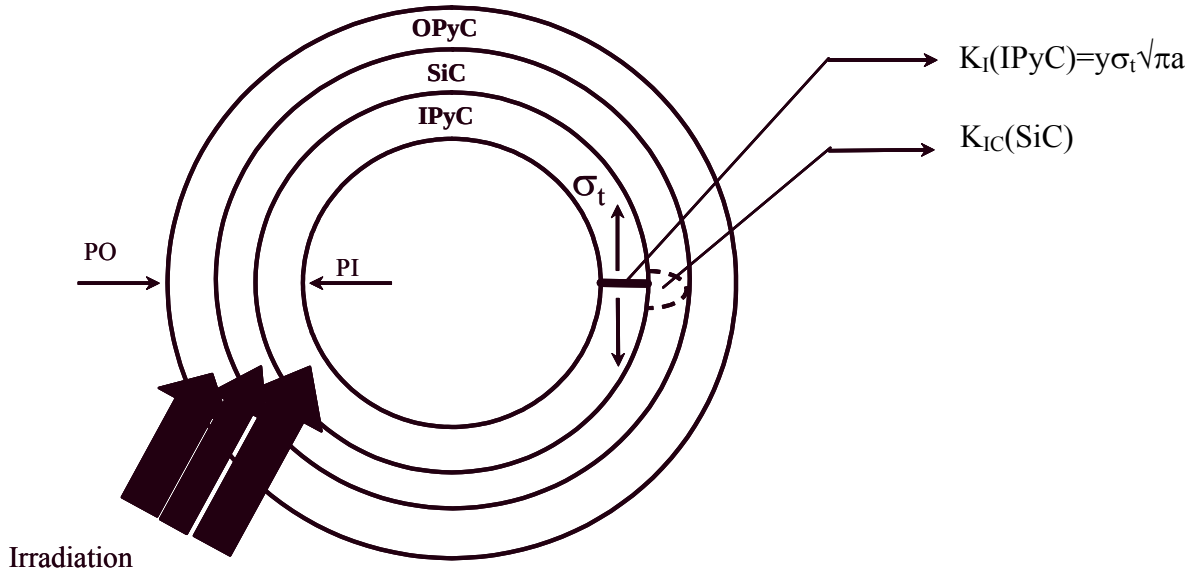


Figure 10. Schematic of cracking of pyrocarbon and SiC layers.

### 3.1 PEBBLE BED FUELING SCHEME

The pebble-bed reactor fueling scheme consists of a number of cycles, typically 10-15, where a particular pebble is fed to the top of the core in a random manner. Once the pebble is introduced it will follow a streamline that is defined, to first order, by the location of entry. The core shape can be approximated by a right circular cylinder with a cone-shaped exit region. Fuel pebbles flow through the system in much the same way that sand flows through an hourglass. When a pebble exits the core its burnup and failure status are checked. If the end of life burnup has not been reached and the pebble contains no failed fuel particles it is recycled to the top of the core where it is introduced once again. However, the ultimate streamline that the pebble follows during a particular pass through the core is independent of the streamline for previous and subsequent passes. Thus, the actual power history for a particular fuel particle is determined by a random process. Unlike the case of the Light Water Reactor where a particular fuel element has a fixed location during each cycle and the fuel manager can shuffle fuel to optimize performance and reliability, the pebble-bed fueling scheme lacks this flexibility. Thus, while from a reliability standpoint it may be advantageous to arrange the exposure such that a fuel element sees a decreasing power density with increased burnup, this is not possible for the pebble-bed reactor. A realistic assessment of pebble-bed fuel reliability thus requires that a fuel performance model be able to accommodate such a fuel management scheme. Due to the fact that the fuel moves through the core in a PBR, the determination of the actual power history for a given fuel particle becomes a complex process. Individual fuel particles must be followed as the pebble in which it resides is cycled through the core. For the analysis presented in this paper, these distributions were obtained by running the VSOP code which was developed in Germany for the pebble-bed system [6]. The VSOP code provides power and neutron flux distributions as a function of both time and position (both axial and radial) within the pebble-bed core. A pebble (hence a particular fuel particle) is randomly re-circulated through the reactor core for the appropriate number of cycles, tracing streamlines determined by the random entry point, thus generating a unique power history for the pebble. At the same time, variables such as neutron flux, power density and coolant temperature are accumulated. Figure 11 shows a schematic of a typical VSOP model for a PBR. The fuel portion of the model is divided into “channels”, in this case 5, each of which is segmented into 9 or 10 “blocks”. Each block is divided into 11 “batches”. The batches within a block have approximately the same volume of fuel + gas space. The burnup is constant within a batch. The steady state core will then consist of a series of blocks within a channel where the burnup distribution as defined by the burnups in the individual batch is defined. The burnup distribution accounts for the fact that individual pebbles in a block may have been through the core a different number of cycles. VSOP provides power peaking factors down to the batch level. Using the results from the VSOP model, Figure 12 shows a typical power history and temperature history for a highly rated fuel particle. As Figure 12 illustrates, the peak power in the particle, while generally decreasing with cycle number due to a reduction in fissionable material, is exposed to a number of cycles where the fuel is “driven” by fresh fuel in the batch. Also, while the average temperature is a generally decreasing function of time, there are cycles where the fuel temperature does not follow this general trend. Such behavior is fundamentally different than what would be the case for a stationary fuel system in a prismatic core and will have a significant effect on fuel reliability.

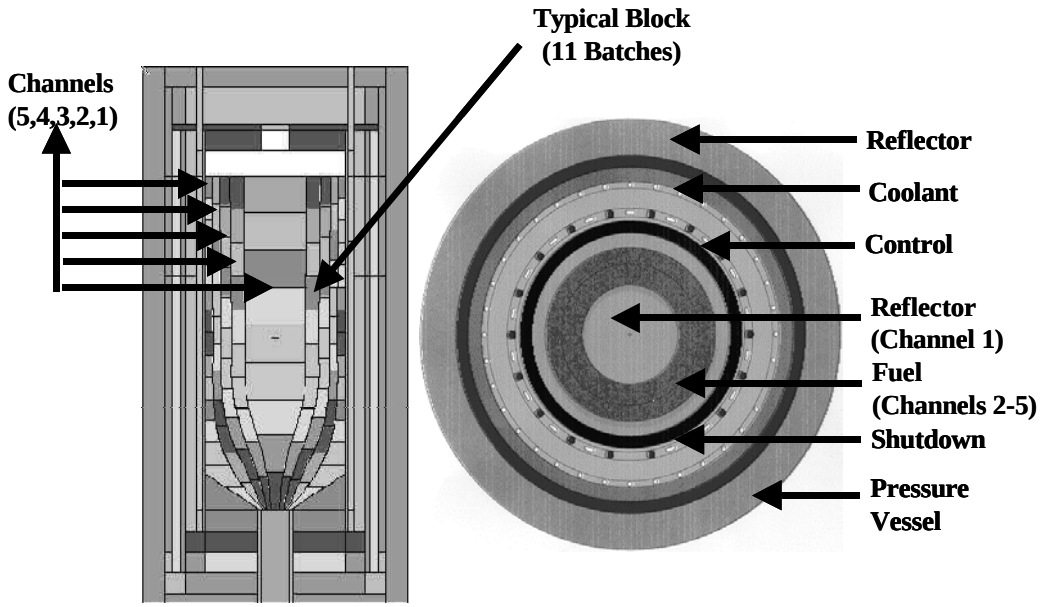


Figure 11. VSOP Model of a typical PBR core.

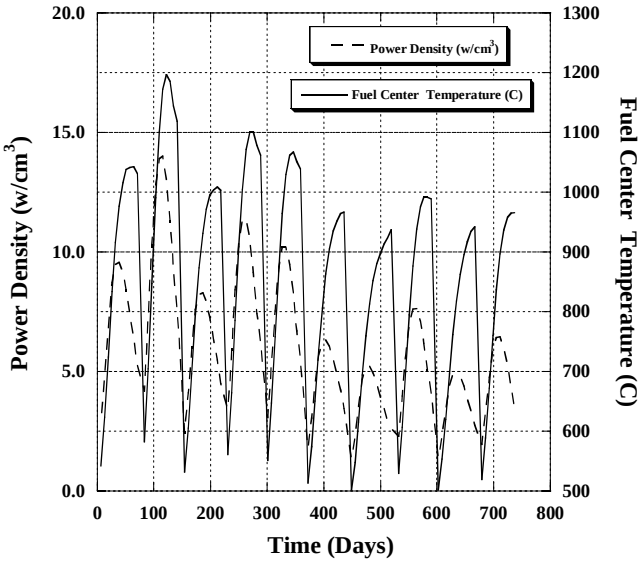


Figure 12. Power density vs. time for typical highly rated particle fuel subjected to a typical pebble-bed reactor power history and fueling scheme.

### 3.2 THE STATISTICAL NATURE OF THE FUEL PROPERTIES AND ENVIRONMENT

As has been discussed above, the generation of appropriate power histories for the fuel requires that fuel pebbles be randomly added at the top of the core for each pass through the bed. What we are most interested in is the probability of failure for the fuel. It is argued that the SiC barrier layer acts as one of the primary boundaries to the release of fission products during an accident. For the SiC layer to serve this purpose the failure probability, among other requirements, must be less than a value on the order of 1 part in $10^6$. In the case of LWR fuel it is possible to inspect each fuel pellet to insure that fabrication requirements (enrichment, dimensions, density, etc.) are met. In the case of the pebble-bed fuel the total fuel load could contain from 360-450,000 pebbles, each containing 11-15,000 fuel particles for a total that could exceed $5 \times 10^9$ particles. While the outside dimensions of the particles can be checked, the individual layer thickness values, particle diameter, and layer mechanical and physical properties cannot be individually verified. Complete inspection requires that the particle be destroyed. For this reason, the dimensional data for actual particles will consist of: (1) a distribution of outside diameter values that have been determined by a go, no-go test to insure that the particle outside diameters are between the specified limits and (2) a set of layer dimensional distributions that will have been determined by inspecting a selected number of particles destructively. Due to the statistical nature of the pebble-bed fueling scheme and the nature of the as-fabricated data for the fuel particles, the estimation of fuel failure probability requires that a statistically significant number of "typical" fuel particles be examined. As a practical matter, this means that at least a million individual particle power histories must be examined for which individual particle properties (dimensions and physical and mechanical) have been assigned by sampling from the property distributions. The modeler, then, is faced with determining (or estimating) the distributions associated with fuel dimensions and, physical and mechanical properties. Since much of the uncertainty in the data will be estimates unless actual data can be obtained, it will be necessary to decide the type of distribution to use for a particular property. The chosen distribution is then used to generate a cumulative probability function from which a normalized property distribution can be derived. It is the normalized distribution that serves as the basis for a Monte Carlo sampling process to determine a set of input files for the fuel modeling system.

## 4.0 EFFECT OF UNCERTAINTY ON FUEL RELIABILITY: RESULTS AND DISCUSSION

The TIMCOAT fuel performance model was used to evaluate the effect of core configuration, fuel design, fuel dimensions and uncertainties, and power history and uncertainty on fuel reliability. Four cases were analyzed, two PBR core configurations and power distributions and, for each of these core designs, the "design" values for the fuel characteristics and the "as-fabricated" fuel characteristics. With respect to the latter, the design fuel specifications generally allow for a wider distribution of characteristics, SiC layer thickness for example, then what turns out to be the actual distribution for the same characteristic.

### 4.1 CORE CONFIGURATIONS AND POWER HISTORIES

For this analysis two core configurations were analyzed. Figure 13 shows an schematic of the two core configurations along with the VSOP mesh that was used for peaking power distribution determination of the equilibrium core. Table 1 shows the characteristics for each core configuration. In the first core, PBR-1, the fuel region is an annulus with an outer solid reflector and an inner "reflector" which consists of un-fueled pebbles. The boundary between the inner reflector and fueled region thus is diffuse with some degree of dilution of both the un-fueled region by fueled pebbles and the fueled region by un-fueled pebbles. As a result of this there is the likelihood that a fresh pebble may find itself in a high flux region which will result in a significantly higher pebble power then for the same burnup but located in an entirely fueled region. The PBR-2 core configuration is fundamentally different than the PBR-1 configuration. In this case the central reflector is now a solid graphite region. For this case there can be no mixing between un-fueled and fueled pebbles. In addition to this difference, the PBR-2 core is designed to operate at a higher gas outlet temperature and a higher average power density. As Table 1 indicates, the maximum power peaking factor for the two configurations is much lower for the PBR-2 configuration than for the PBR-1 configuration. Figures 14 and 15 show the power peaking distribution for the two configurations.

Table 2 shows the design and as-fabricated fuel characteristics. These fuel characteristics are not meant to represent actual fuel characteristics from the current ESKOM-designed PBR but were taken from German experience. Two series of LEU-TRISO fuel particles were manufactured by the German NUKEM plant for irradiation testing under controlled conditions in materials testing reactors. One batch was manufactured in 1981 and was irradiated under a variety of different conditions in several reactors. The so-called "Proof Test" fuel spheres were manufactured in 1988, and eight spheres were irradiated under conditions simulating the High Temperature Modular Reactor (HTR-Modul) conditions in the HFR Petten materials testing reactor. [7,8]

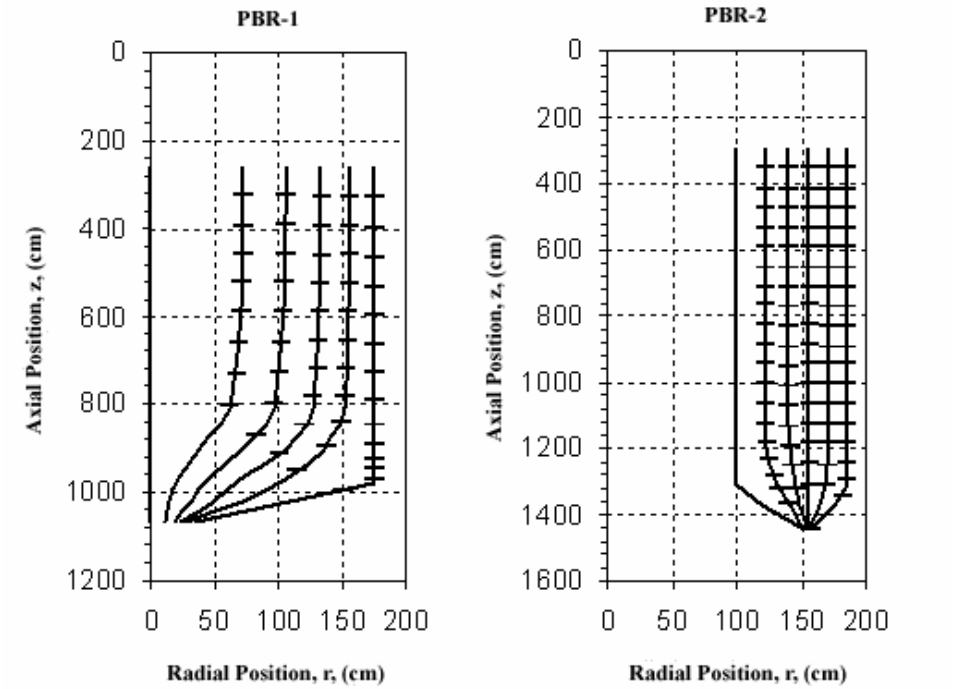


Figure 13. Core configuration and VSOP "mesh" for PBR-1 and PBR-2 core configurations.

Our purpose here is to take use of this fuel design to show simulations in VSOP modeled MPBR cores and to exhibit the effect of fuel optimization. The "Design Specification" column in the table refers to HTR-Modul design values, and the "As Manufactured" column refers to values achieved during manufacture of Type EUO 2308 coated particles.

### 4.1.1 RESULTS-POWER HISTORIES

Figures 16-19 show the power history results for the simulations of the PBR-1 and PBR-2. Figures 16 and 17 show the fast neutron fluence and burnup of a nominal TRISO particle for each of the PBR environments. The PBR-1 core configuration and operation required 10 cycles to complete the required exposure. The PBR-2 configuration required 6 cycles to reach the end of life burnup. The irradiation time is about 750 days for PBR-1 and 1000 days for PBR-2. The end-of-life fluence and burnup depend on the specific path the particle follows. Therefore the fluence and burnup developments shown in these figures are just examples. For the Monte Carlo simulations, each sampled particle will have a specific path-dependent irradiation history. Roughly speaking, the average end-of-life fluence for the particles in PBR-1 and PBR-2 are

$1.9\times10^{21}$n/cm$^2$ and $2.8\times10^{21}$n/cm$^2$, respectively. The end-of-life burnup is between 9% to 10% FIMA. The accumulation of fluence and burnup in each cycle clearly indicates the cosine-shaped power and fast neutron flux distributions in the axial direction of the reactor cores.

Figure 18 shows the power histories of a typical particle for the two reactor cores. Due to the high power peaking factor in the mixing zone of PBR-1, the power history for this configuration and operation shows more fluctuation. The power history in PBR-2 shows a more well behaved decreasing trend through cycles due to the depletion of the fuel.

Table 1. Characteristics for PBR Core Configurations

| Parameter | PBR-1 | PBR-2 |
|---|---|---|
| Core Height (m) | 10.0 | 11.0 |
| Core Radius (m) | 1.75 | 1.85 |
| Thermal Power (MW) | 250 | 400 |
| Coolant | Helium | Helium |
| Core Inlet Temperature (°C) | 450 | 500 |
| Core Outlet Temperature (°C) | 850 | 900 |
| Average Power Density (MW/m$^3$) | 3.652 | 4.777 |
| Max. Power Peaking Factor | 5.27 | 2.74 |
| Min. Power Peaking Factor | 4.44E-5 | 2.70E-5 |
| Coolant Mass Flow Rate (kg/s) | 118.0 | 154.6 |
| No. Pebbles in Core | 360,000 | 451,600 |
| No. Particles per Pebble | 11,000 | 15,000 |
| No. of Cycles | 10 | 6 |
| No. VSOP Blocks | 57 | 93 |
| No. VSOP Batches per Block | 11 (10 effective*) | 7 (6 effective*) |
| Pebble Fuel Zone Radius (mm) | 25.0 | 25.0 |
| Pebble Radius (mm) | 30.0 | 30.0 |

Figure 19 shows the temperature histories at the center of a typical particle corresponding to its irradiation history. Although the coolant inlet and outlet temperatures of PBR-1 are lower than of PBR-2, the fuel temperature in PBR-1 is higher due to the presence of very high local power density regions in the core. As a result, the time averaged fuel temperature in PBR-1 may indeed be higher.

The higher average temperature for PBR-1 may lead to lower stresses in structural layers. The degree of relaxation of stresses is, as was pointed out earlier, dependent on the balance between shrinkage/swelling induced stresses and the ability of creep to relax the stress. A typical set of these stresses are plotted in Figure 20. Note that the stresses are higher early in life for the PBR-2 cases. Additionally, since the PBR-2 configuration has a higher exposure time, the stresses remain in place longer. The ripples of stress curves are created by the thermal cycling as the particle passes through the core.

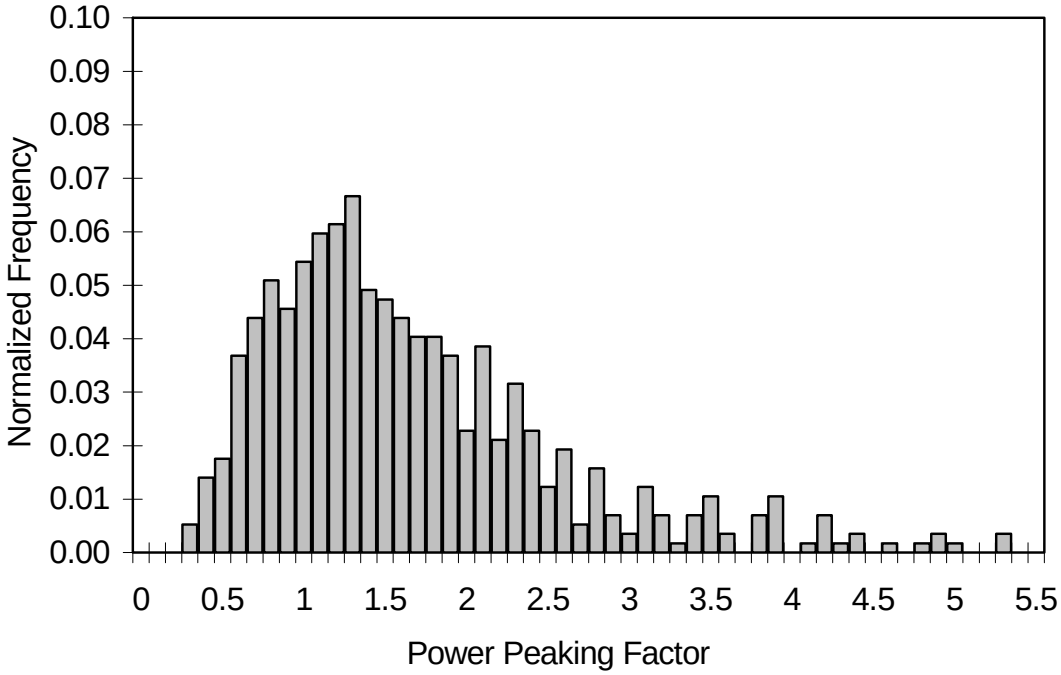


Figure 14. VSOP calculated power peaking factor distribution for the PBR-1 core configuration.

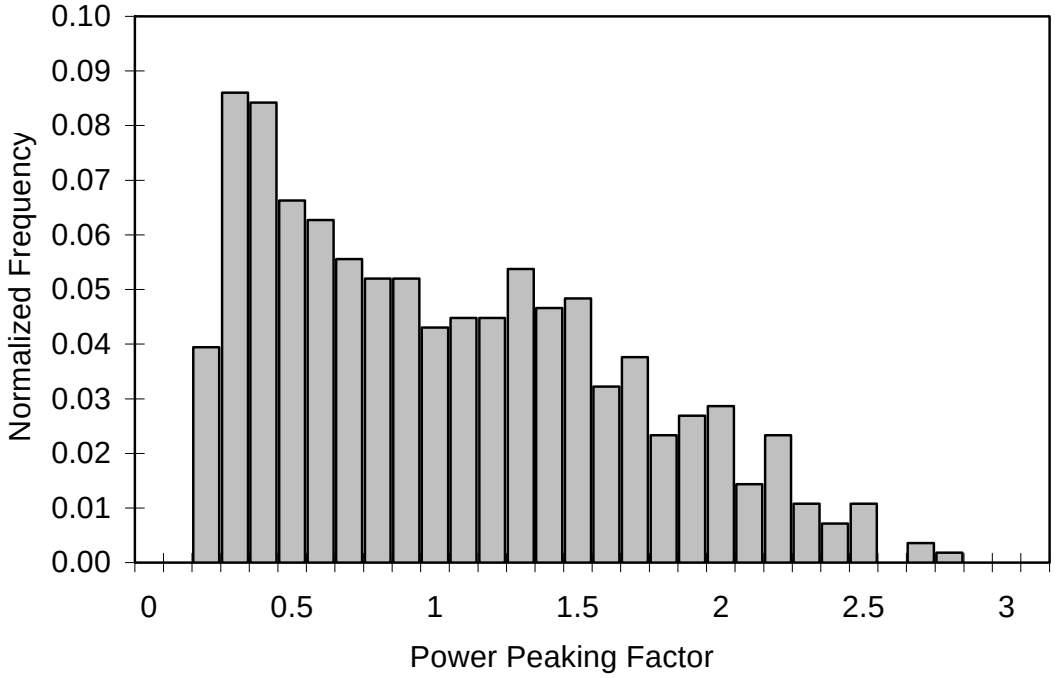


Figure 15. VSOP calculated power peaking factor distribution for the PBR-2 core configuration

Table 2. Specifications for TRISO Fuel Used for Simulations [7,8]

| Parameter | Design Specification | As Manufactured |
|---|---|---|
| Fuel Type | $UO_2$ | $UO_2$ |
| $U^{235}$ Enrichment (%) | $7.8 \pm 0.1$ | † |
| Kernel Diameter (μm) | $500 \pm 20$ | $497 \pm 14.1$ |
| Kernel Density (g/cm$^3$) | $\geq 10.4$ | $10.81 \pm 0.01$ |
| Buffer Thickness (μm) | $90 \pm 18$ | $94 \pm 10.3$ |
| Buffer Density (g/cm$^3$) | $\leq 1.05$ | $1.00 \pm 0.05$ |
| IPyC Thickness (μm) | $40 \pm 10$ | $41 \pm 4.0$ |
| IPyC Density (g/cm$^3$) | $1.90 \pm 0.1$ | Not Measured |
| SiC Thickness (μm) | $35 \pm 4.0$ | $36 \pm 1.7$ |
| SiC Density (g/cm$^3$) | $\geq 3.18$ | 3.20 |
| OPyC Thickness (μm) | $40 \pm 10$ | $40 \pm 2.2$ |
| OPyC Density (g/cm$^3$) | $1.90 \pm 0.1$ | 1.88 |
| IPyC/OPyC $BAF_0$ | $1.058 \pm 0.00543$ | $1.058 \pm 0.00543$ |
| Defective SiC | $\leq 6 \times 10^{-5}$ | $3.5 \times 10^{-5}$ |

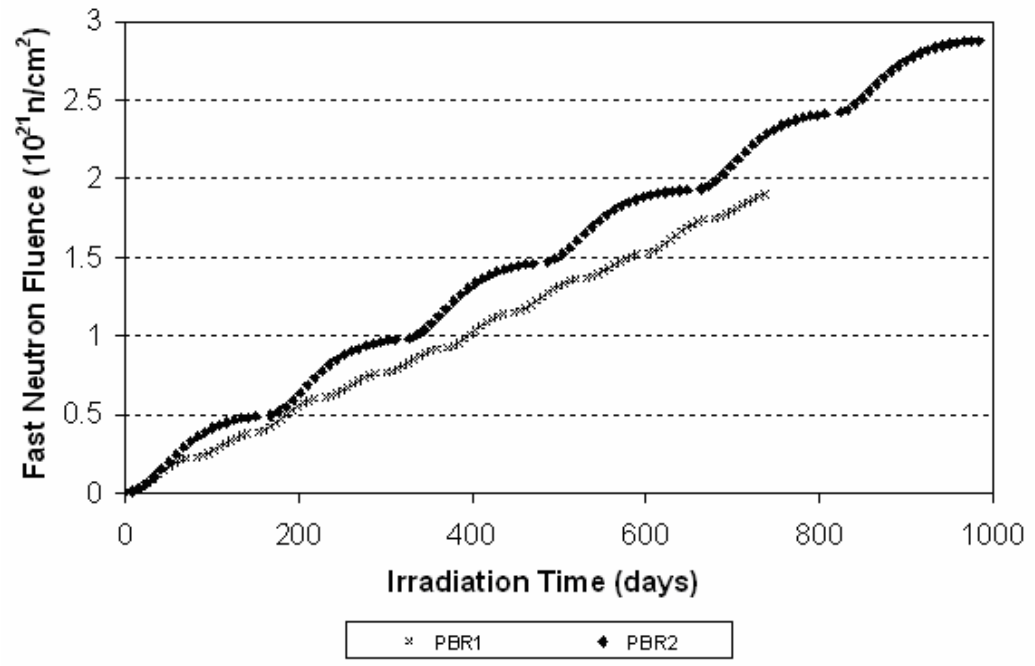


Figure 16. Fast neutron fluence accumulation for Cases PBR-1 and PBR-2.

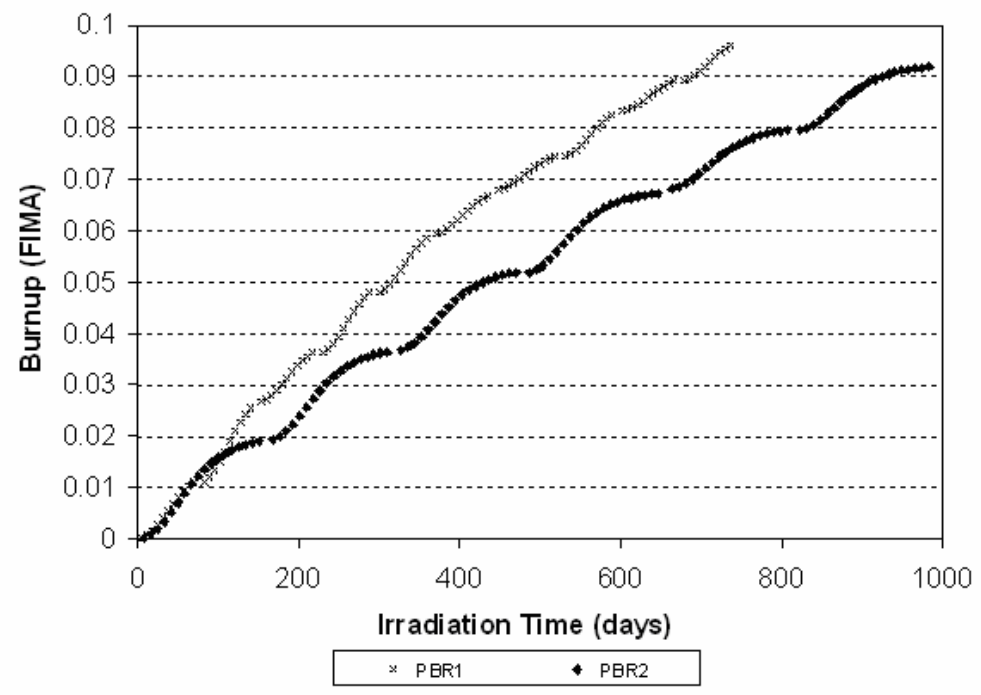


Figure 17. Burnup accumulation for Cases PBR-1 and PBR-2

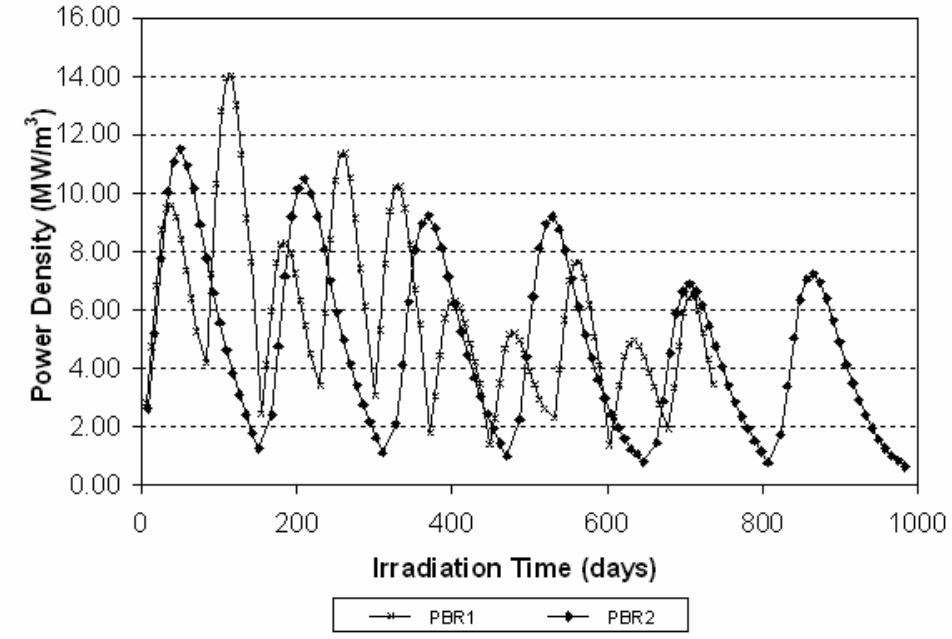


Figure 18. Typical power histories for Cases PBR-1 and PBR-2. Note: These histories are one of up to 10 million histories that were generated as a part of the Monte Carlo simulation process.

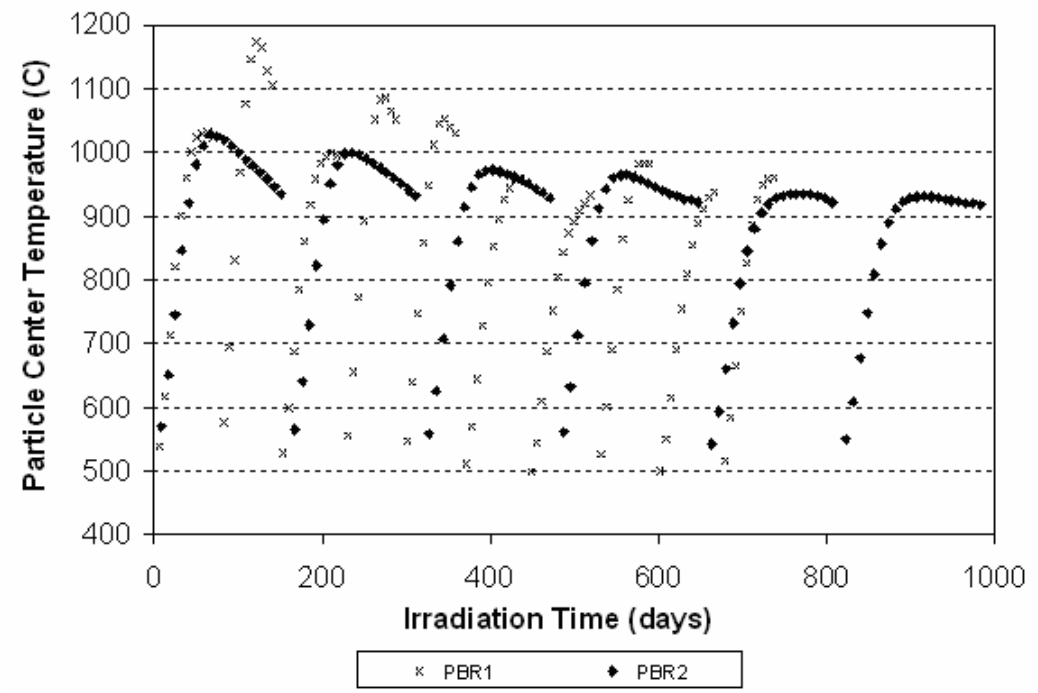


Figure 19. . Typical temperature histories for Cases PBR-1 and PBR-2. Note: These histories are one of up to 10 million histories that were generated as a part of the Monte Carlo simulation process.

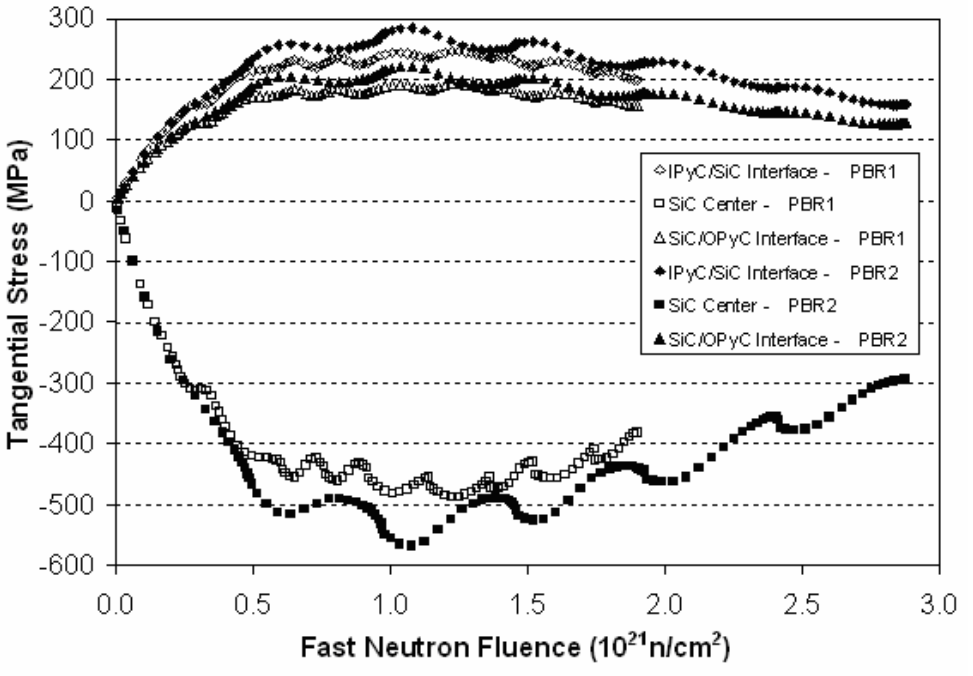


Figure 20. Typical tangential stresses for Cases PBR-1 and PBR-2. Note: These histories are one of up to 10 million histories that were generated as a part of the Monte Carlo simulation process.

Figure 21 shows a typical set of dimensional change rates for the pyrocarbon layers in a PBR-2 case. These data are included to illustrate the non-linearity introduced by the thermal cycling (the fueling paths) and the fluence dependence of the swelling/shrinkage behavior of pyrocarbon.

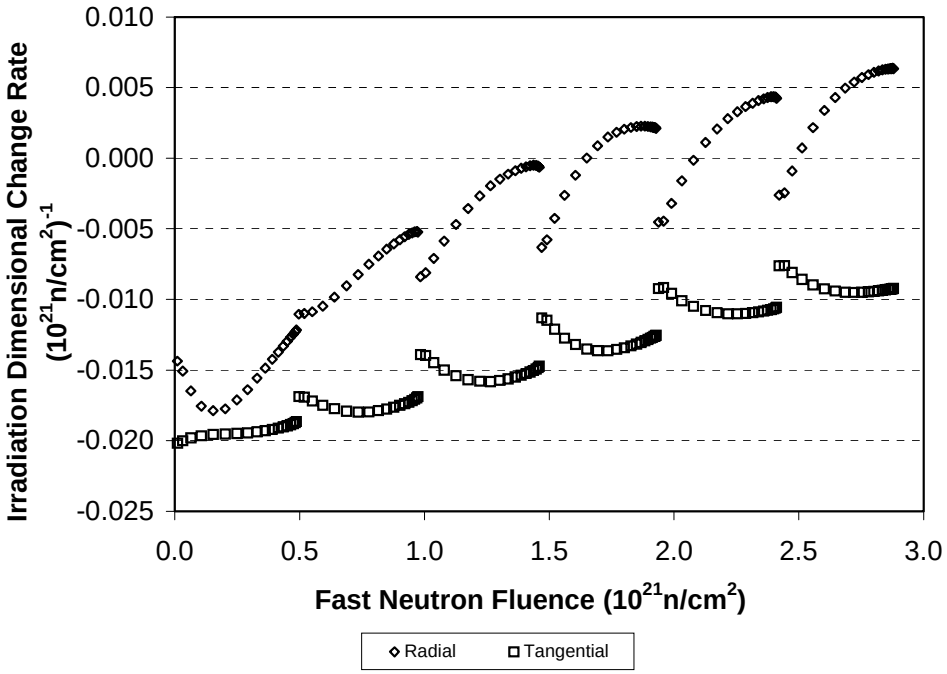


Figure 21. Typical Irradiation induced dimensional change rates of PyC layers in PBR-2. Note: These histories are one of up to 10 million histories that were generated as a part of the Monte Carlo simulation process.

### 4.1.2 RESULTS: FAILURE PROBABILITIES

The reliability of the fuel for the two PBR cases was evaluated using a Monte Carlo simulation in with an initial sample size of 1,000,000. The details of the procedure and choice of distribution characteristics have been described elsewhere [1]. The Monte Carlo simulation included sampling from both fuel dimensions and properties as well as for the fueling scheme. The results of this simulation along with their standard deviations are presented in Table 3 and in Figure 22. The following characteristics of the results are of note:

1. The failure probability of the "design" fuel is higher than the "as-fabricated" fuel.
2. The failure probability of the PBR-2 fuel is higher than the PBR-1 fuel in spite of the fact that the peaking factor distribution for the PBR-1 fuel had a tail with several peaking factors that were much higher then the PBR-2 fuel.
3. In the simulation of one million as fabricated particles in the PBR-1 case, the standard deviation of particle failure probability (0.00555%) is higher than the probability itself (0.00340%), meaning that the prediction is not significantly different from zero.

4. Failure by overpressure did not occur for any of the cases stufied.

Insight into why this might be the case can be gained by noting that the average temperature of the PBR-1 cases are higher than in PBR-2 cases. The higher temperature will allow for a higher creep rate which will promote stress relaxation. With respect to the design vs. as-fabricated comparison, we find that the PyC layer failure probabilities in the as fabricated fuel are a little higher but particle failure probability is much lower for the as-fabricated cases. This is because the failures of the SiC layer is primarily driven by the extreme particle species on the tails of their dimension distributions, and the narrowing of those distributions in as the fabricated fuel particles excludes many of those which might result in SiC failure. Concerning the standard deviation for the PBR-1 case, when the sample number is increased to ten million, the standard deviation decreased to about half of the mean particle failure probability. Also, while the mean value for the failure probability predictions the predictions remain approximately stationary, the standard deviations are reducedt by a factor of the square root of the sample enlargement, in this case, about $\sqrt{10}$ .

Table 3. Failure Predictions for PBR-1 and PBR-2 Cases.

| Case | IPyC Failure | OPyC Failure | SiC Failure | Particle Failure |
|---|---|---|---|---|
| Design Specified in PBR-1 | 34.37% ± 0.388% | 3.66% ± 0.189% | 0.104% ± 0.0286% | 0.104% ± 0.0286% |
| As Fabricated in PBR-1 (1M Cases) | 35.84% ± 0.456% | 3.78% ± 0.196% | 0.00340% ± 0.00555% | 0.00340% ± 0.00555% |
| As Fabricated in PBR-1 (10M Cases) | 35.93% ± 0.149% | 3.80% ± 0.0603% | 0.00394% ± 0.00210% | 0.00394% ± 0.00210% |
| Design Specified in PBR-2 | 52.25% ± 0.498% | 6.91% ± 0.259% | 0.461% ± 0.0766% | 0.461% ± 0.0766% |
| As Fabricated in PBR-2 | 55.41% ± 0.522% | 7.00% ± 0.239% | 0.0645% ± 0.0239% | 0.0645% ± 0.0239% |

## 4.2 DISCUSSION

Before we attempt to rationalize the results of the simulations we must e aware of the boundaries and limitations of this analysis:

1. The analysis, while making use of “real-world” fuel specifications and power histories, does not represent and analysis of a particular fuel. Moreover, while the model has been benchmarked against NPR irradiations and has compared very favorably and the authors believe that the model contains the relevant and necessary physics for the mechanical failure problem, the absolute results should be taken as qualitative and more useful in comparing designs in a relative sense.
2. The analysis deals with failures due to the mechanical fracture of the PyC-SiC-PyC layer by either crack-induced failure or overpressure. There are many other failure scenarios

that may also produce failure. These would include failure due to chemical interaction between fission products and the layers, migration of the fuel kernel into the barrier layers and the presence of as-fabricated defects in the fuel.

3. As of this writing, the current limitation on fluence for the model is $4 \times 10^{21}$ n/cm$^2$ which represents the limit of the PyC radiation damage data base. For operation outside of this limit a linear extrapolation is used. This may or may not be the most appropriate scheme to use.

With the above caveats in mind, Figure 22 shows the cumulative failure probability as a function of irradiation time for the cases studied. The maximum failure probability is about $4.6 \times 10^{-3}$ for the PBR-2 design fuel. The minimum failure probability is approximately $4.0 \times 10^{-5}$ for the as-fabricated PBR-1 fuel. The PBR-2 design case behavior is characteristic of an early failure fraction where the stresses due to shrinkage cannot be relieved by creep due to the lower temperature operation, followed later in life by an increase in failure due to the eventual cracking of SiC initiating from previously cracked PyC that, at the time of PyC cracking, did not result in immediate SiC layer cracking. After initial PyC cracking, continued shrinkage of the PyC caused a gradual increase in SiC crack tip stress intensity until failure occurred. The plateau in cumulative failure probability occurs when the population of particles at risk is eliminated and the remaining particles cannot develop sufficient stress. The failure rate for the as-fabricated PBR-2 cases was much lower then the design case and, in addition, the onset of failures did not occur until much later in life. However, the cumulative failure probability for the PyC layers was approximately the same for each case. In this case, while there was cracking of the PyC layers, the resulting stress concentration was insufficient to cause immediate SiC layer failure. However, a small fraction of these particles began to fail later in life due to the continued buildup of SiC stress intensity as the PyC continued to shrink. The overall lower failure probability of the as-fabricated particles is due to a tighter distribution on the as-fabricated fuel dimensions and properties, as the power history distribution for each particle type was the same.

The PBR-1 failure rates are both much lower overall and the cumulative failure probability exhibits a different shape than for the PBR-2 cases. The reason for this behavior is that at the higher average temperature the ability for the system to relax the stress from PyC shrinkage is enhanced. Thus, for the same set of uncertainties in the design parameter case there are simply fewer “outliers” in the kernel population that would lead to a set of early failures. At the same time, the set of previously PyC cracked kernels is still very significant. Thus there will be a continuous increase in stress concentration at the PyC/SiC interface as burnup increases. However, the ability to relax the stress is still apparent in that the second class of failures, at higher burnup, is much smaller. For the as-fabricated PBR-1 cases the population of at-risk kernels is extremely small and the overall failure probability, in spite of a once again very significant cracked PyC population, remains very low.

## 5.0 CONCLUSIONS

The above analysis illustrates the complexity of the interaction between materials properties and environment in the behavior of coated particle fuel. In the case of LWR fuel, the fuel pellets contact the fuel only at high burnup and remains uncoupled with the cladding until this time. Once fuel/clad contact occurs the chemical/mechanical interaction can lead to cladding

failure. The cladding behaves as a monolith. Overpressure failure is very unlikely. In the case of coated particle fuel this is not the case. The fuel/"clad" contact can only occur at very high temperatures. However, even in the case of fuel contact the interaction is not mechanical but chemical. Thus, the fuel does not participate in the mechanical failure of the layers except to the extent that fission gas cause and increase in pressure or the fission products interact directly. More importantly, the The PyC/SiC/PyC system is a composite system and the behavior of the system is closely coupled to the behavior of the individual layers. As the results of this analysis would seem to show, it is not a forgone conclusion that reducing temperature will result in increased reliability. A balance must be struck between PyC swelling/shrinkage behavior, creep resistance, and operating temperature-at least when addressing failure by mechanical means. It is not even clear that simply assuring that the anisotropy ($BAF_0$) is minimized will lead to increased reliability. The strength (hence creep resistance) of PyC increases with $BAF_0$. This behavior must also be taken into account in coated particle fuel design. At the same time, a high $BAF_0$ will lead to increased shrinkage rates early in life-the very cause of increased stresses. Thus, greater attention must be paid to the assembly of this system. Lastly, the design optimization will involve a significant number of tradeoffs between the expenditure of resources to develop processes that assure a specific set of processes and the expenditure of resources for inspection of the as-fabricated product. The narrowing of the distribution of properties around a selected mean can have more effect on ultimate behavior than the property itself. In this analysis the ultimate failure probability, while quite low, is dominated by outliers in the distributions-both in terms of as-fabricated parameters and power histories. A careful examination of each of the kernels that were predicted to fail showed that they possessed the highest stresses in all cases. They were all outlier in the properties distributions.

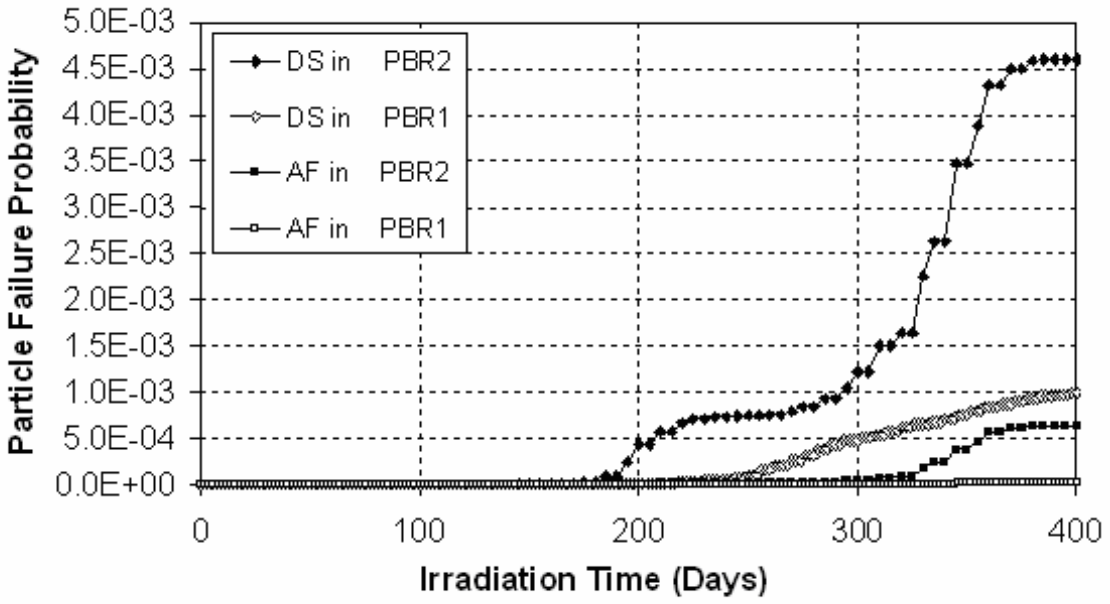


Figure 22. Failure developments for particles in PBR-1 and PBR-2.

## REFERENCES


1. J. Wang, R. G. Ballinger, and H. Maclean, "An Integrated Fuel Performance Model for Coated Particle Fuel", Submitted to Nuclear Technology
2. J. Wang. and R. G. Ballinger, "An Integrated Fuel Performance Model for the Modular Pebble Bed Reactor", ANS Winter Meeting, Reno, NV, November 2001.
3. J. Wang. and R. G. Ballinger, "A Fracture Mechanics Based Failure Model for TRISO Fuel Particles", ANS Winter Meeting, Reno, NV, November 2001.
4. J. Wang and R. G. Ballinger, "The Effect of Design and Uncertainty on Coated particle Fuel Reliability", ANS Summer Meeting, San Diego, June 1-5, 2003
5. J.L. Kaae, "Irradiation-Induced Microstructural Changes in Isotropic Pyrolytic Carbons, Journal of Nuclear Materials, **57**, 82-92 (1975)
6. E. Techert, et al., "V.S.O.P (94) Computer Code System for Reactor Physics and Fuel Cycle Simulation", Forschungszentrum, Julich GmbH (Jul-2897), April 1994.
7. H. Ragoss, "Experimental Safety of the Fuel Elements for Normal and Accident Conditions of the HTR-Modul", INTERATOM 76.00526.9, September 1987
8. H. Nabielek, "Quantitative Evaluation of the Performance of German HTR Fuel under Normal Operating and under Accident Conditions", KFA ISR-IB-19/93, December 1993 (Reprinted August 1999)
9.


## ACKNOWLEDGEMENTS


The authors gratefully acknowledge the support of the US Nuclear Regulatory Commission in the funding of this research.